J. Fluid Mech. (1989), *vol.* 199, *pp.* 495–518
Printed in Great Britain

Symmetry-breaking bifurcations in resonant surface waves

By Z. C. FENG AND P. R. SETHNA
Deparment of Aerospace Engineering and Mechanics, University of Minnesota, Minneapolis, MN 55455, USA

(Received 12 April 1988 and in revised form 12 July 1988)

Surface waves in a nearly square container subjected to vertical oscillations are studied. The theoretical results are based on the analysis of a derived set of normal form equations, which represent perturbations of systems with 1 : 1 internal resonance and with D_4 symmetry. Bifurcation analysis of these equations shows that the system is capable of periodic and quasi-periodic standing as well as travelling waves. The analysis also identifies parameter values at which chaotic behaviour is to be expected. The theoretical results are verified with the aid of some experiments.

1. Introduction

This work is on nonlinear surface waves in a container subjected to vertical periodic oscillations. The earliest work on this subject is by Faraday (1831), and more recent work starts with Benjamin & Ursell (1954). In the last few years, there has been renewed interest in the study of weakly nonlinear phenomena associated with surface waves. The most interesting phenomena, including chaotic behaviour, are due to internal resonance which occurs when the ratios of natural frequencies of two or more modes of motion are near some small positive integers. Miles (1984*a*, *b*) has studied such wave phenomena when two modal frequencies are nearly equal, in the case of circular containers, in the unexcited and horizontally excited cases respectively. He has also studied the case of vertical excitations when the modal frequencies are in the ratio of 1:2 (Miles 1984*c*). This problem has also been studied by Gu & Sethna (1987) and by Holmes (1986).

The case when two modal frequencies are nearly equal, the excitation is vertical and the container is circular, or nearly square, has special fascination owing to the inherent symmetry of the problem. For a circular container, Ciliberto & Gollub (1984) have given some experimental results, and Meron & Procaccia (1986*a*, *b*) have derived amplitude equations, based on symmetry considerations, to provide a theoretical basis for the experimental results. The free oscillations in a nearly square container, when the frequencies are nearly equal, is discussed by Bridges (1987). This study is limited to the study of standing waves.

Our study is motivated by work of Gu & Sethna (1987). In that work, periodic, almost periodic and chaotic wave motions are studied in the case of a rectangular container subjected to vertical sinusoidal motions when the frequencies of two modes are in the ratio of 1:2. The requirement of this frequency ratio, however, makes the fluid height relatively small, which causes excessive energy dissipation which, in turn, suppresses nonlinear phenomena. It is, therefore, not possible to verify the results experimentally. In the case of a nearly square container, on the other hand, all the non-symmetric modes have nearly equal natural frequencies independent of

the fluid depth. Thus, this case is amenable to both a theoretical and an experimental investigation, which is the subject of this work.

Specifically, we derive the normal form equations from the basic equations of fluid motions and thus give explicit formulae for all the parameters in the normal form equations in terms of the physical parameters. We then present a complete bifurcation analysis of the motion and show that the system is capable of periodic standing waves in the form of mixed modes, travelling waves with steady rotations around 'nodal points' of the two linear modes, almost periodic motions in the latter two kinds of waves, and we locate parameter values at which chaotic phenomena are expected to occur. Furthermore, we present results from experiments that verify, with different degrees of accuracy, all the above phenomena.

The discussion given here does not include global bifurcation analysis leading to chaotic phenomena as discussed by Gu & Sethna (1987) and by Holmes (1986) in order to keep the presentation to a reasonable length. A study of such bifurcations, combining the approaches in the above two references, is in progress.

As mentioned earlier, symmetry plays an important role in the analysis. The fourth-order normal form equations, as is well known, represent an equivalence class of dynamical systems depending on the parameter values. They represent normal form equations of very general perturbed Hamiltonian dynamical systems with one–one resonance and with D_4 symmetry. The perturbations are such that the perturbed system still retains $Z_2 \oplus Z_2$ symmetry. It can be shown that the case discussed here is one of 24 distinct cases of such systems. The works of Verhulst (1978), Swift (1988) and the fundamental works of Golubitsky & Stewart (1985, 1986) are relevant references on this subject.

Finally, we mention the work of Simonelli & Gollub (1989) that we have received in a private communication. In their work, which is primarily experimental, they study the same problems discussed here. To the best of our knowledge, none of their conclusions contradict the theoretical or experimental results given here. Their experimental work is done with much more sophisticated techniques and is much more complete than what is given here.

2. Problem formulation and normal form equations

We follow here closely the discussion in Gu & Sethna (1987). Consider a rigid rectangular container filled with an inviscid incompressible fluid subjected to vertical motions $F\cos\nu t$ with respect to a fixed reference frame. We assume that the flow is irrotational and, thus, there exists a potential function $\phi(\boldsymbol{x}, t)$, where $\boldsymbol{x}$ is the position with respect to the container, so that $\nabla\phi = \boldsymbol{V}$, where $\boldsymbol{V}$ is the fluid velocity relative to the container. Furthermore, owing to the assumptions of incompressibility and irrotationally, ϕ satisfies Laplace's equation. The origin of a moving Cartesian reference frame is attached to the container at the undisturbed free surface of the fluid. The cross-section of the container is rectangular of sides a and b and the fluid depth is H. Let the free surface be denoted by $z = \eta(x, y, t)$. If

$$x = a\tilde{x}, \quad y = b\tilde{y}, \quad z = a\tilde{z}, \quad \phi = a^2\left(\frac{g}{a}\right)^{\frac{1}{2}}\tilde{\phi}, \quad \eta = a\tilde{\eta},$$

$$\lambda = \frac{H}{a}, \quad \lambda_1 = \frac{a}{b}, \quad \omega = \frac{\nu}{2\left(\frac{g}{a}\right)^{\frac{1}{2}}}, \quad f = \frac{\nu^2 F}{g}, \quad t = \frac{2\tilde{t}}{\nu} = \frac{\tilde{t}}{\omega\left(\frac{g}{a}\right)^{\frac{1}{2}}},$$

where g is the acceleration of gravity, then dropping tilde signs, we have

$$\phi_{xx}+\lambda_1^2\phi_{yy}+\phi_{zz}=0 \quad \text{for} \quad 0\leqslant x\leqslant 1, \quad 0\leqslant y\leqslant 1, \quad -\lambda\leqslant z\leqslant \eta(x,y,t). \tag{2.1}$$

The boundary conditions are

$$\phi_x=0 \quad \text{on} \quad x=0,1; \qquad \phi_y=0 \quad \text{on} \quad y=0,1; \qquad \phi_z=0 \quad \text{on} \quad z=-\lambda, \tag{2.2}$$

and on the boundary $z=\eta(x,y,t)$

$$\omega\phi_t+\tfrac{1}{2}(\phi_x^2+\lambda_1^2\phi_y^2+\phi_z^2)+(1-f\cos 2t)\,\eta=0, \tag{2.3}$$

$$\omega\eta_t+\phi_x\eta_x+\lambda_1^2\phi_y\eta_y-\phi_z=0, \tag{2.4}$$

and, from the incompressibility of the fluid, we have

$$\int_0^1\int_0^1 \eta(x,y,t)\,dx\,dy=0. \tag{2.5}$$

Let ϵ be a small parameter and let the dimensionless forcing amplitude $f=\epsilon\Delta$ and ϕ and η be of $O(\epsilon^{\frac{1}{2}})$. We obtain a restricted class of asymptotic solutions of system (2.1)–(2.5) in the limit as ϵ tends to zero. A variety of equivalent procedures are available for such analysis; see for instance Gu & Sethna (1987), Bridges (1987) and Kit, Shemer & Miloh (1987). Our analysis is closely related to the last two references. Our solution becomes a two-mode solution of the linearized version of (2.1)–(2.5) when $\epsilon=0$.

Our discussion is limited to the case of a rectangular container which is almost square in cross-section. We therefore take $\lambda_1=1+O(\epsilon)$. If $f=0$ and if we drop all nonlinear terms in (2.1)–(2.5), the solution can be shown to be

$$\phi=\sum_{j,k=0}^{\infty}\tfrac{1}{2}(d_{jk}\,e^{i\omega_{jk}t/\omega}+d_{jk}^*\,e^{-i\omega_{jk}t/\omega})\,\Phi_{jk}(x,y,z), \tag{2.6}$$

where

$$\left.\begin{aligned}\Phi_{jk}(x,y,z)=g_{jk}(z)\,S_{jk}(x,y), \quad \omega_{jk}^2=K_{jk}\tanh(K_{jk}\lambda), \quad K_{jk}^2=\pi^2(j^2+k^2),\\ g_{jk}(z)=\frac{\cosh K_{jk}(\lambda+z)}{\cosh K_{jk}\lambda}, \quad S_{jk}(x,y)=\cos j\pi x\cos k\pi y.\end{aligned}\right\} \tag{2.7}$$

The d_{jk} are arbitrary constants and d_{jk}^* their complex conjugates.

Our interest is in motions when the system is excited sinusoidally in the vertical direction. It is well known that under such excitations the linear modes with frequencies that are nearest to half of the excitation frequency get strongly excited. Since the container is nearly square, if the mode with mode number (m,n) gets excited then the mode with mode number (n,m) will get excited also. Thus for $m\neq n$, two modes get excited simultaneously in this manner. Furthermore, owing to presence of nonlinear terms the modal amplitudes will have time evolution in a slow time $\tau=\epsilon t$. We therefore assume that the problem for $\epsilon\neq 0$ has a solution of the form

$$\begin{aligned}\phi_1(x,y,z,t,\tau)=\frac{1}{2\omega_{mn}}g_{mn}(z)\{&[Z_1(\tau)\,S_{mn}(x,y)+Z_2(\tau)\,S_{nm}(x,y)]\,e^{it}\\ &+[Z_1^*(\tau)\,S_{mn}(x,y)+Z_2^*(\tau)\,S_{nm}(x,y)]\,e^{-it}\},\end{aligned} \tag{2.8}$$

where $Z_1(\tau)$ and $Z_2(\tau)$ are the two complex amplitudes, $Z_1^*(\tau)$ and $Z_2^*(\tau)$ are their complex conjugates and they are determined by the terms neglected in the above analysis.

Let $$\omega=\omega_{mn}+\sigma_0\epsilon, \quad \lambda_1=1+\tfrac{1}{2}\gamma\epsilon, \quad \tau=\tfrac{1}{2}\epsilon t, \tag{2.9}$$

and let $$\eta(x,y,t,\tau,\epsilon)=\epsilon^{\frac{1}{2}}\eta_1(x,y,t,\tau)+\epsilon\eta_2(x,y,t,\tau)+\epsilon^{\frac{3}{2}}\eta_3(x,y,t,\tau)+\ldots. \tag{2.10}$$

The function ϕ depends on the space variables, the time t, the slow time τ and ϵ. We shall see that the expansion of ϕ in a series analogous to (2.10), results in ϕ_2 having a term that is a constant times t. This is not a source of any difficulty since the problem can be thought of as defined on a bounded set in the space variables and a bounded interval in t, since all solutions are periodic in t with a period 2π and defined for all values of the slow time τ. Alternatively, we note that only the derivative of ϕ with respect to the space variable and with respect to t appears in (2.1)–(2.5) and thus the above-mentioned term in t disappears. Thus one can assume expansion of these derivatives in terms of a power series in $\epsilon^{\frac{1}{2}}$ without the occurrence of a linear term in t. For simplicity, we take the former view and regard t to be a bounded interval.

Let $$\phi(x,y,z,t,\tau,\epsilon) = \epsilon^{\frac{1}{2}}\phi_1(x,y,z,t,\tau)+\epsilon\phi_2(x,y,z,t,\tau)+\epsilon^{\frac{3}{2}}\phi_3(x,y,z,t,\tau)+\ldots, \quad (2.11)$$

with $O \leqslant x \leqslant 1, O \leqslant y \leqslant 1, -\lambda \leqslant z \leqslant \eta, O \leqslant t \leqslant 2\pi, -\infty < \tau < +\infty$. We note that

$$\begin{aligned}\eta_t &= \epsilon^{\frac{1}{2}}\eta_{1t}+\epsilon^{\frac{1}{2}}\eta_{1\tau}\frac{\mathrm{d}\tau}{\mathrm{d}t}+\epsilon\left(\eta_{2t}+\eta_{2\tau}\frac{\mathrm{d}\tau}{\mathrm{d}t}\right)+\epsilon^{\frac{3}{2}}\left(\eta_{3t}+\eta_{3\tau}\frac{\mathrm{d}\tau}{\mathrm{d}t}\right)+O(\epsilon^2)\\ &= \epsilon^{\frac{1}{2}}\eta_{1t}+\epsilon\eta_{2t}+\epsilon^{\frac{3}{2}}(\tfrac{1}{2}\eta_{1\tau}+\eta_{3t})+O(\epsilon^2).\end{aligned}$$

Substituting (2.9)–(2.11) into (2.1)–(2.5) and equating coefficients of powers of $\epsilon^{\frac{1}{2}}$, we have a sequence of boundary-value problems in terms of η_j and ϕ_j. The procedure for solving these problems is, by now, standard and will not be given here. We merely remark that in the solution for ϕ_2 there will be spatial modes with mode numbers $(2m,0),(0,2m),(2n,0),(0,2n),(m-n,m+n),(m+n,m-n),(m+n,m+n),(m-n,m-n),(2m,2n),(2n,2m)$. It can be shown that the natural frequencies of these modes are not close to ω_{mn} and thus ϕ_2 can be solved uniquely. With regard to ϕ_3, it is not necessary to solve for it explicitly. For ϕ_3 to be bounded we apply the Fredholm Alternative (see Kit *et al.* 1987 and Bridges 1987) as the solvability conditions to obtain equations for the complex amplitudes Z_1 and Z_2, as follows:

$$\frac{2\sigma_0}{\omega_{mn}}Z_1-\mathrm{i}\frac{\mathrm{d}Z_1}{\mathrm{d}\tau}-\pi_1 Z_1^2 Z_1^*-\pi_2 Z_1 Z_2 Z_2^*-\pi_3 Z_1^* Z_2^2-\tfrac{1}{2}\Delta Z_1^*-\tilde{\gamma}(n\pi)^2 Z_1 = 0, \quad (2.12a)$$

$$\frac{2\sigma_0}{\omega_{mn}}Z_2-\mathrm{i}\frac{\mathrm{d}Z_2}{\mathrm{d}\tau}-\pi_1 Z_2^2 Z_2^*-\pi_2 Z_1 Z_2 Z_1^*-\pi_3 Z_2^* Z_1^2-\tfrac{1}{2}\Delta Z_2^*-\tilde{\gamma}(m\pi)^2 Z_2 = 0, \quad (2.12b)$$

where
$$\tilde{\gamma} = \frac{\gamma}{2K_{mn}^2}\left(1+\frac{K_{mn}^2-\omega_{mn}^4}{\omega_{mn}^2}\lambda\right), \quad (2.13)$$

and where π_1, π_2 and π_3, when neither m nor n is zero, take the form

$$\begin{aligned}\pi_1 = -\omega_{mn}^4\Bigg\{&\frac{1}{128}\Bigg[-\frac{9}{\tanh^6((1+r^2)^{\frac{1}{2}}h)}+\frac{24(1+r^4)}{(1+r^2)^2[\tanh^4((1+r^2)^{\frac{1}{2}}h)]}\\ &-\frac{5}{\tanh^2((1+r^2)^{\frac{1}{2}}h)}+46\Bigg]\\ &+\frac{1}{32[(1+r^2)^{\frac{1}{2}}\tanh((1+r^2)^{\frac{1}{2}}h)]^3}\Bigg[\frac{(3[(1+r^2)^{\frac{1}{2}}\tanh((1+r^2)^{\frac{1}{2}}h)]^2-3+r^2)^2}{\tanh(2h)-2[(1+r^2)^{\frac{1}{2}}\tanh((1+r^2)^{\frac{1}{2}}h)]}\\ &+\frac{(3[(1+r^2)^{\frac{1}{2}}\tanh((1+r^2)^{\frac{1}{2}}h)]^2-3r^2+1)^2}{r\tanh(2rh)-2[(1+r^2)^{\frac{1}{2}}\tanh((1+r^2)^{\frac{1}{2}}h)]}\Bigg]\Bigg\}, \quad (2.14a)\end{aligned}$$

$$\pi_2 = -\omega_{mn}^4 \left\{ \frac{1}{16} \left[\frac{2}{\tanh^4((1+r^2)^{\frac{1}{2}}h)} - \frac{2(1+r^4)}{(1+r^2)^2(\tanh^4((1+r^2)^{\frac{1}{2}}h))} \right.\right.$$

$$\left. - \frac{4}{\tanh^2((1+r^2)^{\frac{1}{2}}h)} + 10 \right] + \frac{1}{16((1+r^2)^{\frac{1}{2}}\tanh((1+r^2)^{\frac{1}{2}}h))^3}$$

$$\times \left[\frac{(3[(1+r^2)^{\frac{1}{2}}\tanh((1+r^2)^{\frac{1}{2}}h)]^2 - 1 - r^2 - 4r)^2}{\sqrt{2}(1+r)\tanh(\sqrt{2}(1+r)h) - 4((1+r^2)^{\frac{1}{2}}\tanh((1+r^2)^{\frac{1}{2}}h))} \right.$$

$$\left. + \frac{(3[(1+r^2)^{\frac{1}{2}}\tanh((1+r^2)^{\frac{1}{2}}h)]^2 - 1 - r^2 + 4r)^2}{\sqrt{2}(1-r)\tanh(\sqrt{2}(1-r)h) - 4((1+r^2)^{\frac{1}{2}}\tanh((1+r^2)^{\frac{1}{2}}h))} \right]$$

$$+ \frac{1}{8((1+r^2)^{\frac{1}{2}}\tanh((1+r^2)^{\frac{1}{2}}h))^3}$$

$$\times \frac{(3[(1+r^2)^{\frac{1}{2}}\tanh((1+r^2)^{\frac{1}{2}}h)]^2 - 1 - r^2)^2}{\sqrt{2}(1+r^2)^{\frac{1}{2}}\tanh(\sqrt{2}(1+r^2)^{\frac{1}{2}}h) - 4((1+r^2)^{\frac{1}{2}}\tanh((1+r^2)^{\frac{1}{2}}h))} \Bigg\}, \tag{2.14b}$$

$$\pi_3 = -\omega_{mn}^4 \left\{ \frac{1}{16} \left[\frac{1}{\tanh^4((1+r^2)^{\frac{1}{2}}h)} - \frac{(1+r^4)}{(1+r^2)^2(\tanh^4((1+r^2)^{\frac{1}{2}}h))} \right.\right.$$

$$\left. \left. + \frac{2}{\tanh^2((1+r^2)^{\frac{1}{2}}h)} + \right] \right\}, \tag{2.14c}$$

where $r = n/m$ and $h = m\pi\lambda$. We note that the above formulae are not valid for two-dimensional motions, i.e. when $n = 0$ or $m = 0$ (see Verma & Keller 1962). When $n = 0$, they take values

$$\pi_1 = -\omega_{m0}^4 \left(\frac{1}{16} + \frac{3}{32\tanh^2(h)} + \frac{3}{8\tanh^4(h)} - \frac{9}{32\tanh^6(h)} \right), \tag{2.15a}$$

$$\pi_2 = -\omega_{m0}^4 \left(\frac{5}{4} - \frac{1}{2\tanh^2(h)} + \frac{(3\tanh^2(h) - 1)^2}{2\tanh^3(h)(\sqrt{2}\tanh\sqrt{2}h - 4\tanh(h))} \right), \tag{2.15b}$$

$$\pi_3 = -\omega_{m0}^4 \left(\frac{1}{8} + \frac{1}{4\tanh^2(h)} \right). \tag{2.15c}$$

Letting $Z_1 = r_1 e^{i\theta_1}$ and $Z_2 = r_2 e^{i\theta_2}$,

$$\sigma = \frac{4\sigma_0}{\Delta\omega_{mn}} - \frac{\tilde{\gamma}K_{mn}^2}{\Delta}, \quad \beta = \frac{\tilde{\gamma}[(n\pi)^2 - (m\pi)^2]}{\Delta}, \quad d = \frac{2d_{mn}}{\Delta},$$

$$\tau = \frac{2\tilde{\tau}}{\Delta}, \quad r_1 = (\tfrac{1}{2}\Delta)^{\frac{1}{2}}a_1, \quad r_2 = (\tfrac{1}{2}\Delta)^{\frac{1}{2}}a_2,$$

we have the basic equations in normal form

$$\dot{a}_1 = (-d + \sin 2\theta_1)a_1 - \pi_3 a_1 a_2^2 \sin(2\theta_2 - 2\theta_1), \tag{2.16a}$$

$$\dot{\theta}_1 = -(\sigma - \beta) + \cos 2\theta_1 + \pi_1 a_1^2 + \pi_2 a_2^2 + \pi_3 a_2^2 \cos(2\theta_2 - 2\theta_1), \tag{2.16b}$$

$$\dot{a}_2 = (-d + \sin 2\theta_2)\, a_2 - \pi_3 a_2 a_1^2 \sin(2\theta_1 - 2\theta_2), \tag{2.16c}$$

$$\dot{\theta}_2 = -(\sigma + \beta) + \cos 2\theta_2 + \pi_1 a_2^2 + \pi_2 a_1^2 + \pi_3 a_1^2 \cos(2\theta_1 - 2\theta_2), \tag{2.16d}$$

where $a_1 \neq 0, a_2 \neq 0$ and where the dot stands for differentiation with respect to $\tilde{\tau}$. Here following Miles (1984*c*) and Gu & Sethna (1987), we introduce the damping term $d = 2d_{mn}/\Delta$, where d_{mn} can be calculated from the formulas given in Miles (1967).

All our results are based on equations (2.16). These equations depend on six parameters: σ, β, d, π_1, π_2 and π_3. Of these parameters π_1, π_2 and π_3 depend on mode numbers, their ratio r and the depth parameter $h = m\pi\lambda$. The normal form equations (2.16) actually represent an entire equivalence class of dynamical systems (see Swift 1988). We now restrict (2.16) by restricting π_1, π_2 and π_3 to values that represent surface waves in a fluid. Explicit calculations show that for $n \neq 0$ and $h > 1$ and $r > 0.13$, the following inequalities hold:

$$\pi_1 < 0, \quad \pi_3 < 0, \quad \pi_1 + \pi_2 + \pi_3 < 0, \quad \pi_1 - \pi_2 - \pi_3 > 0, \quad \pi_1 + \pi_2 - \pi_3 > 0, \tag{2.17}$$

and these inequalities hold independently of the specific mode numbers themselves.

The restrictions $h > 1$ and $r > 0.13$ are justifiable and, in fact, necessary. When $0 < h < 1$, the fluid depth is small with the result that the dissipative effects are strong; and, when these effects are strong, they tend to suppress nonlinear phenomena. When $0 < r < 0.13$, we have fairly large mode numbers and it can be shown that when the mode numbers are large, the values of the natural frequencies of several modes are close to each other. The result is that the phenomena predicted by the two-mode analysis given here will occur for extremely small intervals of the parameter σ and thus the analysis is not very useful. The case when $n = 0$, i.e. when $r = 0$, at first sight appears to be a case that we have eliminated in the above discussion. As discussed earlier the values of π_j as given in (2.14) when $r \to 0$ are, however, not the same values as those given in (2.15). Again, when $h > 1$ we find the values of the π as given in (2.15) satisfy (2.17). We thus need to study only one case with the π satisfying (2.17). In addition to the combination of the π as given in (2.28), we give, for reference, the following ratios of the π that occur frequently in the subsequent analysis:

$$p = \frac{-\pi_1 - \pi_2 + \pi_3}{\pi_1 - \pi_2 + \pi_3}, \quad q = \frac{\pi_1 + \pi_2 + \pi_3}{-\pi_1 + \pi_2 + \pi_3}, \tag{2.18}$$

and we note that $0 < p < 1$ and $q > 1$.

3. Bifurcation analysis

We now discuss the solutions of (2.16) and interpret them in terms of surface waves. Constant solutions of (2.16) represent periodic waves at approximately the linear modal frequency. There are values of system parameters when there are no waves, i.e. $a_1 = a_2 = 0$, or when there are waves in a single mode, i.e. either a_1 or a_2 is zero, or when there are waves in a mixed mode, when neither a_1 nor a_2 is zero. We shall see that the mixed-mode solutions are of more than one type, generating physically different phenomena.

Period solutions of (2.16) represent modal motions occurring at approximately the linear modal frequency with amplitude modulations at a frequency that is on a slow timescale. The waves thus generated are quasi-periodic waves. We shall show that

such wave motions occur only when the motion is with mixed modes and we shall also show that there are two types of such mixed-mode motions. The amplitude-modulated motions often lead to chaotic behaviour.

The system (2.16) has a total of six parameters: d, σ, β, π_1, π_2 and π_3. For a given fluid height, mode numbers and basic dimensions of the container, π_1, π_2 and π_3 are constants and satisfy (2.17). For given fluid-container dimensions and forcing amplitude, d is a constant. We perform our bifurcation analysis in terms of σ and β. For fixed mode numbers, the parameter σ is proportional to the difference of detuning of the external excitation frequency and the deviation of aspect ratio from one, and inversely proportional to the excitation amplitude, while β is proportional to the deviation of the aspect ratios of the container cross-section from one, and inversely proportional to the excitation amplitude. Since the deviation of the aspect ratio also represents the detuning between the modal frequencies, β can also be interpreted as a detuning parameter for 'internal resonance' of the system.

The above-mentioned large variety of physical phenomena occur as the parameters σ and β are varied and the transition from one phenomenon to another occurs at a bifurcation. The vast majority of the bifurcations are local and codimension one. There are, however, four combinations of σ and β where local bifurcations of more than one codimension occur. We first discuss the codimension-one bifurcations.

The basic equations in normal form are (2.16). These equations are not valid when a_1 or a_2 or both are zero. We, therefore, write them in the Cartesian form. Let

$$x_1 = a_1\cos\theta_1, \quad y_1 = a_1\sin\theta_1, \quad x_2 = a_2\cos\theta_2, \quad y_2 = a_2\sin\theta_2. \tag{3.1}$$

Then

$$\dot{x}_1 = -dx_1 + (1+\sigma-\beta)\,y_1 - y_1[\pi_1(x_1^2+y_1^2)+\pi_2(x_2^2+y_2^2)] - 2\pi_3 x_1 x_2 y_2 + \pi_3 y_1(x_2^2-y_2^2), \tag{3.2a}$$

$$\dot{y}_1 = (1-\sigma+\beta)\,x_1 - dy_1 + x_1[\pi_1(x_1^2+y_1^2)+\pi_2(x_2^2+y_2^2)] + \pi_3 x_1(x_2^2-y_2^2) + 2\pi_3 y_1 x_2 y_2, \tag{3.2b}$$

$$\dot{x}_2 = -dx_2 + (1+\sigma+\beta)\,y_2 - y_2[\pi_1(x_2^2+y_2^2)+\pi_2(x_1^2+y_1^2)] - 2\pi_3 x_1 x_2 y_1 + \pi_3 y_2(x_1^2-y_1^2), \tag{3.2c}$$

$$\dot{y}_2 = (1-\sigma-\beta)\,x_2 - dy_2 + x_2[\pi_1(x_2^2+y_2^2)+\pi_2(x_1^2+y_1^2)] + \pi_3 x_2(x_1^2-y_1^2) + 2\pi_3 y_2 x_1 y_1, \tag{3.2d}$$

We note the following symmetries of system (3.2):

(i) D_4 symmetry when $\beta = 0$, i.e. if $(x_1(t), y_1(t), x_2(t), y_2(t))$ is a solution, then $(x_1(t), y_1(t), -x_2(t), -y_2(t))$, $(-x_1(t), -y_1(t), x_2(t), y_2(t))$, $(-x_1(t), -y_1(t), -x_2(t), -y_2(t))$ and $(x_2(t), y_2(t), x_1(t), y_1(t))$ are also solutions of (3.2).

(ii) $Z_2 \oplus Z_2$ symmetry when $\beta \neq 0$, i.e. if $(x_1(t), y_1(t), x_2(t), y_2(t))$ is a solution, then $(-x_1(t), -y_1(t), x_2(t), y_2(t))$, $(x_1(t), y_1(t), -x_2(t), -y_2(t))$ and $(-x_1(t), -y_1(t), -x_2(t), -y_2(t))$ are also solutions of (3.2).

(iii) Parameter symmetry (Swift 1988), i.e. if β is replaced by $-\beta$ and (x_2, y_2, x_1, y_1) are replaced by (x_1, y_1, x_2, y_2), the system is unchanged. This makes it possible to restrict the analysis to $\beta > 0$ without loss of generality.

We also need to consider an intermediate form of (3.2) as follows:

$$\dot{x}_1 = -(d+\pi_3 a_2^2\sin 2\theta_2)\,x_1 + (1+\sigma-\beta+\pi_3 a_2^2\cos 2\theta_2 - \pi_2 a_2^2)\,y_1 - \pi_1 y_1(x_1^2+y_1^2), \tag{3.3a}$$

$$\dot{y}_1 = (1-\sigma+\beta+\pi_3 a_2^2\cos 2\theta_2 + \pi_2 a_2^2)\,x_1 - (d-\pi_3 a_2^2\sin 2\theta_2)\,y_1 + \pi_1 x_1(x_1^2+y_1^2), \tag{3.3b}$$

$$\dot{a}_2 = (-d+\sin 2\theta_2)\,a_2 - 2\pi_3 x_1 y_1 a_2 \cos 2\theta_2 + \pi_3 a_2(x_1^2-y_1^2)\sin 2\theta_2, \tag{3.3c}$$

$$\dot{\theta}_2 = -\sigma-\beta+\cos 2\theta_2+\pi_1 a_2^2+\pi_2(x_1^2+y_1^2)+\pi_3(x_1^2-y_1^2)\cos 2\theta_2+2\pi_3 x_1 y_1 \sin 2\theta_2. \tag{3.3d}$$

System (3.3) has Z_2 symmetry in the variables x_1 and y_1.

We shall discuss our results in terms of bifurcation sets and bifurcation diagrams (Chow & Hale 1982). Bifurcation sets are graphs in the (σ,β)-plane on which the system equations become degenerate, and bifurcation diagrams, which for simplicity we describe in terms of amplitudes a_1 and a_2 only (ignoring the θ_1 and θ_2 variables) as a function of the detuning of σ for fixed values of β. We shall see that there are four intervals of the parameter β in each of which the bifurcation diagrams are qualitatively different.

We show that the bifurcation sets are either straight lines or curves as in figure 1. The points at which they intersect, in most cases, have not special significance, since the intersecting lines or curves represent bifurcations of different solutions. There are, however, four points, marked A, B, C and D, which represent more complicated phenomena of more than one codimension. Phenomena associated with these points will be discussed after the discussion of codimension-one local bifurcation.

3.1. *The zero solution*

The stability of the zero solution (3.2) is determined by the eigenvalues of the Jacobian matrix of (3.2) evaluated at the origin, and they are

$$\lambda_{1,2} = -d \pm (1-(\sigma+\beta)^2)^{\frac{1}{2}}, \quad \lambda_{3,4} = -d \pm (1-(\sigma-\beta)^2)^{\frac{1}{2}}.$$

For $d \neq 0$, we note that the system can be degenerate only through the eigenvalues going through zero, i.e. no Hopf bifurcations are possible. This can also be seen from the $Z_2 \oplus Z_2$ symmetry of the system.

If we let $\beta_1 = (1-d^2)^{\frac{1}{2}}$, then

$$\sigma_1 = \beta_1+\beta, \quad \sigma_2 = -\beta_1+\beta, \quad \sigma_3 = \beta_1-\beta, \quad \sigma_4 = -\beta_1-\beta \tag{3.4}$$

are the bifurcation sets at which one or the other eigenvalue has a simple zero. For these values of the parameters, one of the eigenvalues is a simple zero, leading to codimension-one bifurcation on a one-dimensional centre manifold; all the bifurcations are pitchfork bifurcation because of the above-mentioned symmetry. The lines in (3.4) intersect at A, B and C where we have codimension-two bifurcations on a two-dimensional centre manifold determined by the simple double-zero eigenvalue of (3.2) at the origin. We shall show below that the bifurcations σ_1, σ_2, σ_3 and σ_4 generate, through pitchfork bifurcations, periodic motions in one or the other of the single modes.

3.2. *One-mode motion*

In this case, we refer to system (3.3) and consider the solution $x_1 = y_1 = 0$ and a_2 and θ_2 satisfying

$$\pi_1 a_2^2 = (\sigma+\beta)-\cos 2\theta_2 \quad \text{and} \quad \sin 2\theta_2 = d.$$

We have expressions for the bifurcation diagram

$$a_2 = ((\sigma-\sigma_3)/\pi_1)^{\frac{1}{2}} \quad \text{and} \quad a_2 = ((\sigma-\sigma_4)/\pi_1)^{\frac{1}{2}}.$$

They are shown as OM3 and OM4 on bifurcation diagrams in figures 2–4, since they represent one-mode motions and they arise in bifurcations σ_3 and σ_4. Since for each

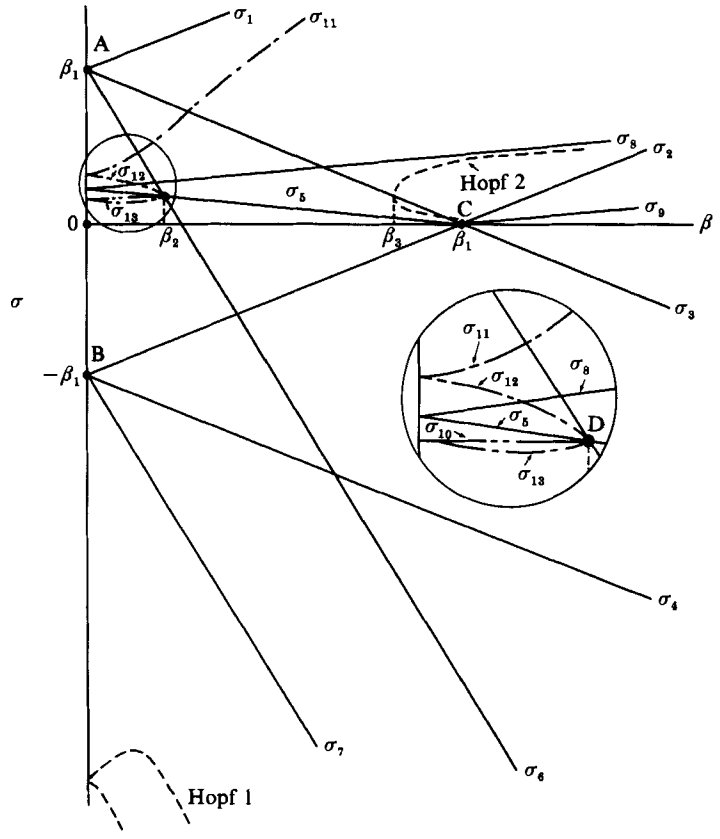

FIGURE 1. Bifurcation set for (1,0), (0,1) modes, infinite fluid depth, damping coefficient $d = 0.1$ ($\beta_1 = 0.99$), except for the Hopf bifurcation where $d \to 0$. The types of bifurcation are: pitchfork (——), Hopf (– – –), saddle-node (— · —) and transcritical (— · · —).

a_2, θ_2 can take two values differing by π, we have in fact four one-mode periodic solutions.

The stability of these solutions are determined by the eigenvalues of the Jacobian matrix of the system (3.3) computed at the constant solution. They can be shown to be the roots of

$$\lambda^2 + 2d\lambda - (\pm 4\pi_1 a_2^2 \beta_1) = 0 \tag{3.5}$$

and

$$\lambda^2 + 2d\lambda + D = 0, \tag{3.6}$$

where

$$D = -1/\pi_1^2\{(\pi_3 - \pi_2 + \pi_1)\sigma + (\pm\beta_1 - \beta)(-\pi_3 + \pi_2 + \pi_1)\}$$
$$\times\{(\pi_3 + \pi_2 - \pi_1)\sigma \pm \beta_1(-\pi_3 - \pi_2 + \pi_1) + \beta(\pi_3 + \pi_2 + \pi_1)\}. \tag{3.7}$$

Again, since $d \neq 0$, the instability of these solutions cannot occur through a Hopf bifurcation. The stability of the solution $a_1 = 0, a_2 \neq 0$ is indicated on the bifurcation diagrams figures 2–4.

Instability of the solutions as determined by (3.5) and (3.6) occurs through a zero eigenvalue when $D = 0$. It can be shown that bifurcations from OM3 occur at

$$\sigma_5 = p(\beta_1 - \beta), \quad \sigma_6 = \beta_1 - q\beta, \tag{3.8}$$

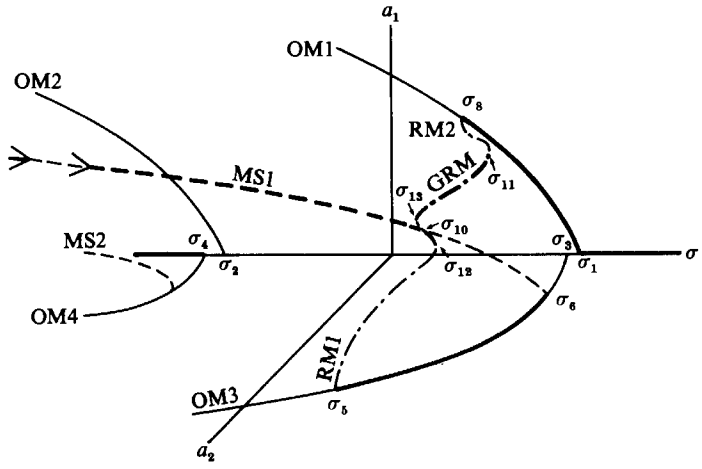

FIGURE 2. Bifurcation diagram for $0 < \beta < \beta_2$ (not to scale). The branches are: pure one-mode (——), rotational wave (— · —), standing wave (– – –). Thick lines denote stable motions and thin lines unstable motions. Hopf bifurcations are denoted by →—.

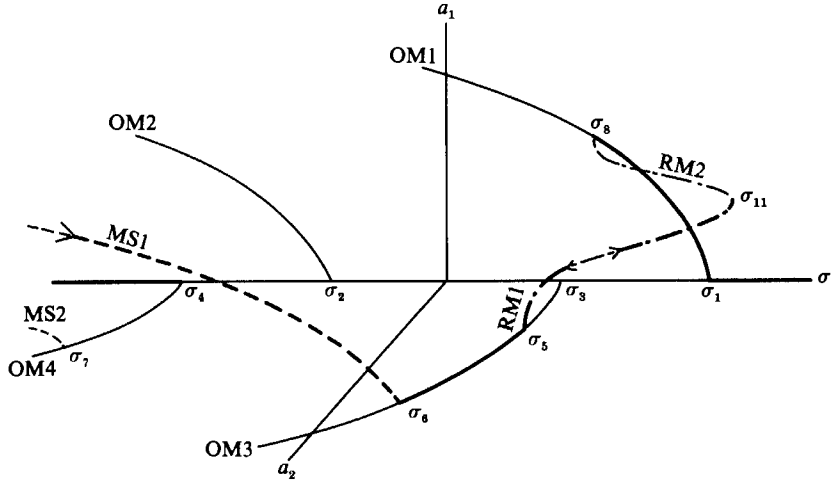

FIGURE 3. Bifurcation diagram for $\beta_2 < \beta < \beta_1$ (not to scale). The branches are: pure one-mode (——), rotational wave (— · —), standing wave (– – –). Thick lines denote stable motions and thin lines unstable motions. Hopf bifurcations are denoted by →—. If $\beta_2 < \beta < \beta_3$, there is no Hopf bifurcation on branch RM1.

where p and q are defined in (2.29). When these bifurcations coalesce, i.e. when $\sigma_5 = \sigma_6$,

$$\beta = \beta_2 = -\frac{\pi_1 - \pi_2 - \pi_3}{2\pi_3}\beta_1, \tag{3.9}$$

the corresponding σ is $\sigma = p(\beta_1 - \beta_2)$. At $(p(\beta_1 - \beta_2), \beta_2)$, we have a codimension-two point, point D, which we discuss later. We note that $\sigma_5 > \sigma_6$ if $\beta > \beta_2$, $\sigma_5 < \sigma_6$ if $\beta < \beta_2$ and $\sigma_6 < \sigma_3$ if $\beta > \beta_1$. These features are shown on the bifurcation diagrams figures 2–4.

In a similar manner a pitchfork bifurcation can be shown to occur from OM4. It is

$$\sigma_7 = -\beta_1 - q\beta. \tag{3.10}$$

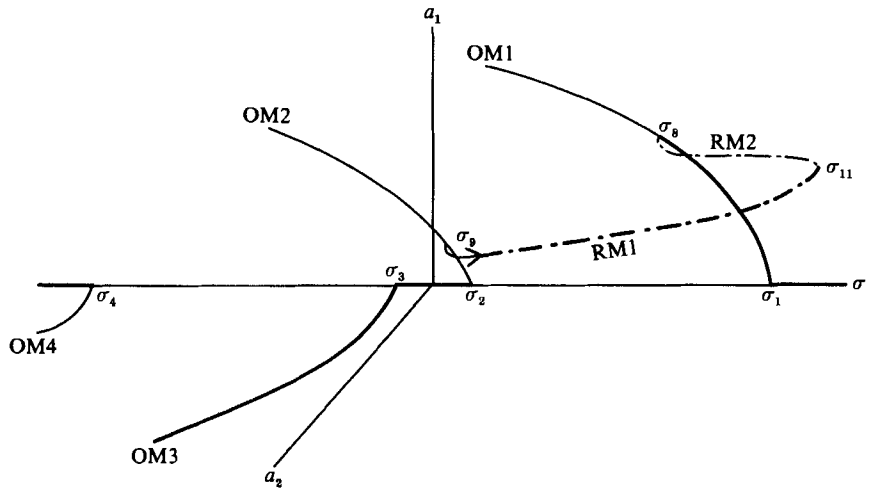

FIGURE 4. Bifurcation diagram for $\beta > \beta_1$ (not to scale). The branches are: pure one-mode (——), rotational wave (—·—). Thick lines denote stable motions and thin lines unstable motions. Hopf bifurcations are denoted by →—.

Similar analysis can be done when $a_2 = 0$, and we have one-mode motions arising from σ_1 and σ_2 as follows:

$$a_1 = ((\sigma-\sigma_1)/\pi_1)^{\frac{1}{2}}, \quad a_1 = ((\sigma-\sigma_2)/\pi_1)^{\frac{1}{2}}.$$

They are shown as OM1 and OM2 on figures 2–4. A study of the stability of these solutions in turn generates pitchfork bifurcations when $\sigma = \sigma_8$ and $\sigma = \sigma_9$ with

$$\sigma_8 = p(\beta+\beta_1), \quad \sigma_9 = p(\beta-\beta_1). \tag{3.11}$$

Note that σ_5 exists only for $\beta < \beta_1$, while σ_9 exists only for $\beta > \beta_1$. All these bifurcations are indicated on figure 1.

We shall now discuss the mixed-mode motions that arise from σ_5–σ_9.

3.3. *Mixed-mode motions*

For the study of mixed modes, it is necessary to study (2.27) in its complete generality. Even the study of its constant solutions, for all values of the parameters, presents considerable difficulty. Some of the mixed-mode solutions arise from the bifurcation of single-mode solutions. It can be shown that the constant solutions that bifurcate from σ_6 and σ_7 have the surprising property that $\theta_1 = \theta_2$, i.e. they are in-phase, while those that bifurcate from σ_5, σ_8 and σ_9 do not have this property. Furthermore, this property is global. We shall see below that these two categories of constant solutions also represent physically different kinds of mixed-mode phenomena.

Instead of extrapolating from the local behaviour at σ_5–σ_9, we treat (2.27) directly and confirm the above observation about θ_1 and θ_2. The constant solutions of (2.27) satisfy

$$\begin{bmatrix} 0 & 0 & 0 & -\pi_3\sin(2\theta_2-2\theta_1) \\ -1 & 1 & \pi_1 & \pi_2+\pi_3\cos(2\theta_2-2\theta_1) \\ 0 & 0 & \pi_3\sin(2\theta_2-2\theta_1) & 0 \\ -1 & -1 & \pi_2+\pi_3\cos(2\theta_1-2\theta_2) & \pi_1 \end{bmatrix} \begin{bmatrix} \sigma \\ \beta \\ a_1^2 \\ a_2^2 \end{bmatrix} = \begin{bmatrix} d-\sin 2\theta_1 \\ -\cos 2\theta_1 \\ d-\sin 2\theta_2 \\ -\cos 2\theta_2 \end{bmatrix}, \tag{3.12}$$

and σ, β, a_1^2 and a_2^2 are uniquely determined in terms of d, θ_1 and θ_2 provided

$$2\pi_3^2 \sin^2(2\theta_2 - 2\theta_1) \neq 0. \tag{3.13}$$

This leads immediately to the two distinct cases.

3.3.1. *In-phase, mixed-mode motions*

We first note that if $\sin(2\theta_1 - 2\theta_2) = 0$, the condition that $d > 0$ requires that $\cos(2\theta_1 - 2\theta_2) = 1$, and $\theta_1 = \theta_2$. System (2.27) then has constant solutions determined by

$$\sin 2\theta_1 = \sin 2\theta_2 = d, \tag{3.14a}$$

$$-(\sigma - \beta) + \cos 2\theta_1 + \pi_1 a_1^2 + \pi_2 a_2^2 + \pi_3 a_2^2 = 0, \tag{3.14b}$$

$$-(\sigma + \beta) + \cos 2\theta_2 + \pi_1 a_2^2 + \pi_2 a_1^2 + \pi_3 a_1^2 = 0. \tag{3.14c}$$

Solutions of (3.14) give two branches of the in-phase solution. It will be seen that these solutions, as distinct from more general solutions, represent standing waves of a distinctive character. Denoting these mixed-mode standing wave solutions by MS1 and MS2, their amplitude and phase satisfy

$$a_1 = \left(\frac{\sigma - \sigma_j}{\pi_1 + \pi_2 + \pi_3}\right)^{\frac{1}{2}}, \quad \theta_1 = \tfrac{1}{2}\sin^{-1} d, \quad j = 6, 7,$$

$$a_2 = \left(\frac{\sigma - (\pm\beta_1) - q\beta}{\pi_1 + \pi_2 + \pi_3}\right)^{\frac{1}{2}}, \quad \theta_2 = \tfrac{1}{2}\sin^{-1} d.$$

It is not difficult to see that branch MS1 bifurcates from branch OM3 at σ_6, while branch MS2 bifurcates from OM4 at σ_7. They are shown on figure 2 and figure 3, while on figure 4, σ_6 and σ_7 are out of the range of the diagrams.

The stability of these in-phase solutions, as well as those of the more general mixed-mode solutions to be discussed later, leads to the study of the roots of a quartic with coefficients that are functions of the appropriate constant solutions a_1^2 and a_2^2, θ_1 and θ_2, as they depend on σ, β and d. A general stability analysis proves to be very cumbersome and we, therefore, here and in the next case, discuss our results in the limit when d is small, which is the case that is expected to include the most interesting phenomena.

We follow here Sethna & Bajaj (1978). It can be shown that the system vector field (3.2) can be written as the sum of the gradient of $-\frac{1}{2}d(x_1^2 + y_1^2 + x_2^2 + y_2^2)$ and a vector field derived from the Hamiltonian

$$\begin{aligned} H = {} & \tfrac{1}{2}(1 + \sigma - \beta) y_1^2 - \tfrac{1}{2}(1 - \sigma + \beta) x_1^2 + \tfrac{1}{2}(1 + \sigma + \beta) y_2^2 - \tfrac{1}{2}(1 - \sigma - \beta) x_2^2 \\ & - \tfrac{1}{4}\pi_1[(x_1^2 + y_1^2)^2 + (x_2^2 + y_2^2)^2] \\ & - \tfrac{1}{2}\pi_2(x_1^2 + y_1^2)(x_2^2 + y_2^2) - \tfrac{1}{2}\pi_3[(x_1 x_2 + y_1 y_2)^2 \\ & - (x_1 y_2 - y_1 x_2)^2]. \end{aligned} \tag{3.15}$$

We note that the constant solutions of the system equations for $d = 0$ and $d \to 0$, approach each other. Furthermore, from the structure of the equations, if λ is an eigenvalue for the variational system for any constant solution when $d = 0$, then the eigenvalue for $d \neq 0$, but $d \to 0$, will be $\lambda - d$. What is important is that when $d = 0$, the eigenvalues have special properties for linear constant-coefficient Hamiltonian systems: if λ is an eigenvalue, then $-\lambda$, λ^* and $-\lambda^*$, where $*$ denotes complex conjugate, are also eigenvalues.

With the above remarks in mind, we pursue the following analysis when $d = 0$ and interpret the results for d small. The quartic determining the stability has a factor d in the coefficient of the cubic and linear term, and thus the eigenvalues of the reduced Hamiltonian system when $d = 0$ satisfy

$$\lambda^4 + \alpha_2 \lambda^2 + \alpha_0 = 0, \tag{3.16}$$

where

$$\alpha_2 = -4[\pm\pi_1(a_1^2 + a_2^2) + 2a_1^2 a_2^2 \pi_3(\pi_1 - \pi_2 - \pi_3)], \tag{3.17}$$

$$\alpha_0 = 16a_1^2 a_2^2(\pi_1 - \pi_2 - \pi_3)(\pi_1 + \pi_2 - \pi_3 \pm 2\sigma\pi_3), \tag{3.18}$$

where the plus sign is for MS1 and minus sign is for MS2.

When $\alpha_0 = 0$, we have a bifurcation point on branch MS1. We denote this bifurcation by σ_{10}; it is, for $d \neq 0$, transcritical, and is a constant

$$\sigma_{10} = \frac{-\pi_1 - \pi_2 + \pi_3}{2\pi_3}, \tag{3.19}$$

and since $\sigma < \sigma_6$, we note that σ_{10} occurs only for $0 < \beta < \beta_2$. For the branch MS2, since $\sigma < \sigma_7 < -1$, α_0 can be shown to be negative, and thus no bifurcation of any kind is possible on this branch.

We also examine MS1 for Hopf bifurcations. It can be shown that the condition $\alpha_2^2 - 4\alpha_0 = 0$ implies a double pair of pure imaginary roots for the Hamiltonian system, and in the limit as d tends to zero, a pair of pure imaginary roots with transversality property, lead to Hopf bifurcations. The value of β for this to occur is

$$\beta_{\text{Hopf}} = (\pi_1 - \pi_2 - \pi_3)\left(\left(\frac{\sigma - \beta_1}{\pi_1 + \pi_2 + \pi_3}\right)^2 - \frac{f(\sigma)}{2(\pi_1 - \pi_2 - \pi_3)}\right)^{\frac{1}{2}}, \tag{3.20}$$

where

$$f(\sigma) = \frac{\pi_3(\pi_2 + \pi_3)\,C(\sigma) + (\pi_1 + \pi_2 + \pi_3)}{\pi_3^2}$$
$$\pm \frac{1}{\pi_3^2}\{(\pi_1 + \pi_2 + \pi_3)[-\pi_3^2(\pi_1 - \pi_2 - \pi_3)\,C^2(\sigma) + 2\pi_3(\pi_2 + \pi_3)\,C(\sigma) + \pi_1 + \pi_2 + \pi_3]\}^{\frac{1}{2}} \tag{3.21}$$

and

$$C(\sigma) = \frac{2(\sigma\beta_1 - 1)}{\pi_1 + \pi_2 + \pi_3}. \tag{3.22}$$

In figure 1, the curve marked Hopf 1 shows the above Hopf bifurcation curve. It is computed in the limit $d \to 0$. Numerical calculation of the fourth-order system of differential equations, using AUTO (a subroutine package for the bifurcation analysis of autonomous systems of ordinary differential equations by Eusebius Doedel) confirms the occurrence of these Hopf bifurcations.

3.3.2. *General mixed-mode solutions*

Since $\sin(2\theta_1 - 2\theta_2) \neq 0$, (3.12) can be used to solve for σ, β, a_1^2 and a_2^2 in terms of d, θ_1 and θ_2:

$$\sigma = \frac{(-\pi_1 - \pi_2 + \pi_3)(\sin 2\theta_2 - \sin 2\theta_1)}{2\pi_3 \sin(2\theta_2 - 2\theta_1)}, \tag{3.23a}$$

$$\beta = \frac{2d[\pi_2 - \pi_1 + \pi_3 \cos(2\theta_2 - 2\theta_1)] + (\pi_1 - \pi_2 - \pi_3)(\sin 2\theta_2 + \sin 2\theta_1)}{2\pi_3 \sin(2\theta_2 - 2\theta_1)}, \tag{3.23b}$$

$$a_1^2 = \frac{d - \sin 2\theta_2}{2\pi_3 \sin(2\theta_2 - 2\theta_1)}, \tag{3.23c}$$

$$a_2^2 = \frac{\sin 2\theta_1 - d}{2\pi_3 \sin(2\theta_2 - 2\theta_1)}. \tag{3.23d}$$

We shall show that the above equations can be combined into a single quartic, the roots of which give the solutions of this general case.

We first introduce

$$\sigma' = \frac{2\sigma\pi_3}{-\pi_1 - \pi_2 + \pi_3}, \quad d' = \frac{-2d\pi_3}{\pi_1 - \pi_2 - \pi_3}, \quad \alpha = \frac{-\pi_1 + \pi_2}{\pi_3}, \quad \gamma = \frac{2\beta\pi_3}{\pi_1 - \pi_2 - \pi_3}. \tag{3.24}$$

Then it can be shown that

$$\sigma' = \frac{\cos(\theta_2 + \theta_1)}{\cos(\theta_2 - \theta_1)}, \quad \gamma = \frac{2\sin(\theta_2 + \theta_1)\cos(\theta_2 - \theta_1) - d'(\alpha + \cos(2\theta_2 - 2\theta_1))}{\sin(2\theta_2 - 2\theta_1)}. \tag{3.25a, b}$$

If $x = \tan(\theta_2 - \theta_1)$, then

$$\cos(2\theta_2 - 2\theta_1) = \frac{1 - x^2}{1 + x^2}, \quad \sin(2\theta_2 - 2\theta_1) = \frac{2x}{1 + x^2}, \quad \cos^2(\theta_2 - \theta_1) = \frac{1}{1 + x^2}. \tag{3.26}$$

Then substituting (3.26) into (3.25b) and using the expression for σ' in (3.25a), we get the following quartic in x:

$$f(x) = (\alpha - 1)^2 d'^2 x^4 + 4(\alpha - 1) d' \gamma x^3 + [4\gamma^2 + 2(\alpha^2 - 1) d'^2 - 4] x^2 + 4(\alpha + 1) d' \gamma x + 4\sigma'^2 + (\alpha + 1)^2 d'^2 - 4 = 0. \tag{3.27}$$

The real roots of (3.27) when substituted in (3.26) give $\cos(2\theta_2 - 2\theta_1)$ in terms of σ', d' and γ. When these expressions are in turn substituted into (3.23a, b), we get $\sin 2\theta_1$ and $\sin 2\theta_2$ and finally a_1^2 and a_2^2 are determined from (3.23c) and (3.23d).

From (3.23c, d and a), we have

$$a_1^2 + a_2^2 = \frac{2\sigma}{\pi_1 + \pi_2 - \pi_3}, \tag{3.28}$$

and since $\pi_1 + \pi_2 - \pi_3 > 0$, these branches exist only for $\sigma > 0$. Furthermore, there is a maximum value of $\sigma' = \sigma'_{\max}$ so that all branches have $\sigma' < \sigma'_{\max}$, and thus the solution of the general case of mixed-mode solution occurs on a finite interval for σ.

We note that as $x \to 0$ in (3.27), $4\sigma'^2 + (\alpha + 1)^2 d'^2 - 4 \to 0$ too, and since $\sigma > 0$ and using (3.23), we have

$$\sigma \to \frac{\pi_3 - \pi_2 - \pi_1}{2\pi_3}(1 - d^2)^{\frac{1}{2}} = \sigma_{10}, \tag{3.29}$$

and thus the general mixed-mode solutions pass through σ_{10} (here evaluated for $d \neq 0$) which is transcritical.

The general mixed-mode solutions arise from one-mode solutions σ_5, σ_8 and σ_9 and as discussed above, as $x \to 0$ in (3.27) the solution approaches that for the in-phase solution. Thus the general mixed-mode solution passes through σ_{10}. Up to this point the bifurcation diagram has evolved with the toplogy of a tree. This is not true of the general mixed-mode solutions. The bifurcation diagram for these solutions, based on numerical calculations are sketched in figures 2–4. The figures show solutions that are

in agreement with the above observation regarding the finite interval of σ on which these solutions occur. We note the saddle-node behaviour of these solutions. The saddle node can be determined by solving for the parameter values at which (3.27) has double roots, i.e. when $f(x) = 0$ and $f'(x) = 0$. In figure 1 we show bifurcation sets for saddle-node bifurcations σ_{11}, σ_{12} and σ_{13}. They are computed for $d = 0.1$. They are also shown on figures 2–4. In figure 2, σ_{12} and σ_{13} are shown on opposite sides of σ_{10}. It is not impossible that they may both occur between σ_5 and σ_{10} for some other value of d. It can be shown that if $\beta = 0$, i.e. for $\gamma = 0$, $\sigma_{13} \to \sigma_{10}$ and the bifurcation at σ_{10} which is, in general transcritical, becomes a pitchfork bifurcation.

To study the bifurcations of these general mixed-mode solutions we again revert to the case when $d \to 0$. The quartic (3.27) then becomes, in the original variables,

$$\left[\left(\frac{2\pi_3\beta}{\pi_1-\pi_2-\pi_3}\right)^2-1\right]x^2+\left(\frac{2\pi_3\sigma}{\pi_1+\pi_2-\pi_3}\right)^2-1=0. \tag{3.30}$$

The two solutions that are lost in this process can be recovered by studying (3.27) for $d = 0$ by again considering $\sin(2\theta_1-2\theta_2) = 0$ but this time with $\theta_1 = 0, \theta_2 = \frac{1}{2}\pi$ and $\theta_1 = \frac{1}{2}\pi, \theta_2 = 0$, and which gives respectively

$$a_1^2 = \frac{\sigma}{\pi_1+\pi_2-\pi_3}-\frac{\beta-(\pm1)}{\pi_1-\pi_2+\pi_3}, \quad a_2^2 = \frac{\sigma}{\pi_1+\pi_2-\pi_3}+\frac{\beta-(\pm1)}{\pi_1-\pi_2+\pi_3}. \tag{3.31}$$

The two expressions in (3.31) are approximations, respectively, of the branches arising from σ_5 and σ_8 when $d \to 0$. We denote these mixed-mode solutions as RM1 and RM2 respectively since they represent, as will be shown later, rotating travelling waves and are mixed-mode solutions.

The two solutions represented by the roots of (3.30) are

$$a_1^2 = \frac{\sigma}{\pi_1+\pi_2-\pi_3}-\frac{\beta}{\pi_1-\pi_2-\pi_3}, \quad a_2^2 = \frac{\sigma}{\pi_1+\pi_2-\pi_3}+\frac{\beta}{\pi_1-\pi_2-\pi_3}, \tag{3.32a, b}$$

and

$$\tan(\theta_2-\theta_1) = \pm\left(\frac{1-\sigma'^2}{\gamma^2-1}\right)^{\frac{1}{2}}. \tag{3.32c}$$

They approximate as $d \to 0$ the two branches of the mixed-mode solution as it passes through σ_{10}.

We indicate on figure 2 the entire damped curve between σ_{11} and σ_{12} as GRM since it represents rotating waves of a more general nature and it occurs as a mixed mode. As $d \to 0$, $\sigma_{13} \to \sigma_{10}$, σ_{11} and $\sigma_{12} \to \infty$ and the two branches from σ_{10} are as represented by (3.32).

The stability of the above four solutions is again determined by the roots of

$$\lambda^4+\alpha_2\lambda^2+\alpha_0 = 0, \tag{3.33}$$

$$\alpha_2 = \pm4\pi_1(a_1^2-a_2^2)+8a_1^2a_2^2(\pi_1-\pi_2+\pi_3)\pi_3, \tag{3.34}$$

$$\alpha_0 = 16a_1^2a_2^2(\pi_1+\pi_2-\pi_3)(-\pi_1+\pi_2+\pi_3-(\pm2\beta\pi_3)), \tag{3.35}$$

where the plus and minus signs correspond to RM1 and RM2 respectively, and in the case GRM we have

$$\alpha_2 = \frac{2}{\pi_3}\left[\left(\frac{2\sigma\pi_3}{-\pi_1-\pi_2+\pi_3}\right)^2(\pi_1-\pi_2+\pi_3)-\left(\frac{2\beta\pi_3}{-\pi_1+\pi_2+\pi_3}\right)^2(-\pi_1+\pi_2+\pi_3)+2\pi_2\right], \tag{3.36}$$

$$\alpha_0 = -\frac{4[(\pi_3-\pi_1)^2-\pi_2^2}{\pi_3^2}\left[\left(\frac{2\beta\pi_3}{-\pi_1+\pi_2+\pi_3}\right)^2-1\right]\left[\left(\frac{2\sigma\pi_3}{-\pi_1-\pi_2+\pi_3}\right)^2-1\right]. \quad (3.37)$$

The stability of these branches are as shown in figures 2–4.

Furthermore it can be shown that Hopf bifurcations are possible only on RM1 and the corresponding value of σ is as follows:

$$\sigma_{\text{Hopf}} = \frac{(\pi_1+\pi_2-\pi_3)(\pm 16C-32\beta\pi_3(\pi_2+\pi_3-\beta\pi_3)+\pi_2^2+\pi_3^2-\pi_1^2)^{\frac{1}{2}}}{4\sqrt{2}\,\pi_3(\pi_1-\pi_2+\pi_3)}, \quad (3.38)$$

where

$$C = \{[(\pi_3^2-\pi_2^2)^2-\pi_1^2](-2\beta\pi_3-\pi_1+\pi_2+\pi_3)(-2\beta\pi_3+\pi_1+\pi_2+\pi_3)\}^{\frac{1}{2}}. \quad (3.39)$$

We observe that, when $-2\beta\pi_3+\pi_1+\pi_2+\pi_3 < 0$, C in (3.39) is imaginary. Thus there is no Hopf bifurcation if

$$\beta < \beta_3 = \frac{\pi_1+\pi_2+\pi_3}{2\pi_3}. \quad (3.40)$$

In figure 1, the curve marked Hopf 2 shows the above Hopf bifurcation. Again it is computed in the limit $d \to 0$.

3.4. *Codimension-two bifurcations*

We shall call a bifurcation a codimension-two bifurcation when the system behaviour near the denegerate bifurcation point can be understood in terms of two parameters, and they may or may not be associated with the linearized system equations.

The codimension-two points are the points A, B, C and D in figure1, and they occur on the boundaries of the intervals $0 < \beta < \beta_2$, $\beta_2 < \beta < \beta_1$ and $\beta > \beta_1$ and the two parameters are σ and β. In the case of A, B and C, the centre manifold is two-dimensional and arises from a simple double zero eigenvalue. The unfolding of these critical points is available in the literature. In Guckenheimer & Holmes (1983) there is a complete discussion of the case of two pairs of pure imaginary eigenvalues without resonance. The results given there can be shown to be directly applicable to our cases, except, in our cases, they are valid for both positive and negative values of the variables. It is not difficult to show that in the case of points A and B, we have the case I b treated in Guckenheimer & Holmes with the time reversed in the case of A. (Specifically, we have these results with μ_1, μ_2, b, c and d in Guckenheimer & Holmes as follows:

$$\mu_1 = \pm(\Delta\sigma+\Delta\beta), \quad \mu_2 = \pm(\Delta\sigma-\Delta\beta), \quad b = c = \frac{\pi_2+\pi_3}{\pi_1} > 1,$$

$$d = 1, \quad d-bc = 1-\left(\frac{\pi_2+\pi_3}{\pi_1}\right)^2 < 0,$$

where $\Delta\sigma = \sigma \mp \beta_1, \Delta\beta = \beta$.) In the case of C, we can show that we have the case VII a. (Specifically, with μ_1, μ_2, b, c and d in Guckenheimer & Holmes as follows:

$$\mu_1 = \Delta\sigma-\Delta\beta, \quad \mu_2 = -(\Delta\sigma+\Delta\beta), \quad b = \frac{\pi_2-\pi_3}{\pi_1} < 0,$$

$$c = -b > 0, \quad d = -1, \quad d-bc = -1+\left(\frac{\pi_2+\pi_3}{\pi_1}\right)^2 < 0,$$

where $\Delta\sigma = \sigma, \Delta\beta = \beta-\beta_1$.) As is well known, such codimension-two analysis at times leads to insights into global bifurcations. We expect some global bifurcations at these points when the entire vector field is Hamiltonian. To understand the global

bifurcations, however, requires the effect of higher-order terms which are beyond the scope of this work.

In the case of D, the situation is quite different. The centre manifold in this case is only one-dimensional and corresponds to a simple zero eigenvalue. The complicated behaviour at D arises partially from the fact that at D the zero eigenvalue does not have transversal behaviour. When $\sigma > \sigma_{10}$ and $\beta = \beta_2$, the eigenvalue approaches zero as $\sigma \to \sigma_{10}$ and for $\sigma < \sigma_{10}$ becomes positive again. A detailed analysis of this critical point is beyond the scope of this work. We expect that it would involve the determination of an approximation to the centre manifold up through terms of order eight. The codimension-two behaviour would arise from the degeneracies in the higher-order terms. Specifically, we expect the polynomial approximation to the flow rate on the centre manifold to be of ninth order. The coefficients of the polynomial are expected to be functions of σ and β taking values near $\sigma = \sigma_{10}$ and $\beta = \beta_2$. Some of these coefficients would be linear in σ and β. When they are zero, they would generate bifurcations σ_5, σ_6 and σ_{10} represented by straight lines; while others would be nonlinear in σ and β and, when they are zero, would generate σ_{12} and σ_{13}. The general behaviour near D can be summarized, on the basis of the separate codimension-one analysis, as follows: The critical eigenvalue remains negative in the sector between σ_5 and σ_6 for both $\beta > \beta_2$ and $\beta < \beta_2$ and is otherwise positive. The number of critical points are one, three, five, nine, seven and seven, respectively, as one goes through open sets around D, starting with the open set in the sector between σ_6 and σ_5 for $\beta > \beta_2$ and going counterclockwise through the seven sectors around D. In the above discussion, we count fixed points that have the same amplitudes a_1 and a_2 but phases θ_1 and θ_2 different by π separately. These fixed points do not appear separately on figures 2–4.

4. Physical interpretation

The several kinds of motion discussed above have, in many cases, simple physical interpretations. The fluid surface η can be expressed as

$$\eta = a_1 \sin(t+\theta_1)\cos(m\pi x)\cos(n\pi y) + a_2 \sin(t+\theta_2)\cos(n\pi x)\cos(m\pi y). \tag{4.1}$$

Nodal lines or curves, for standing waves, occur when $\eta = 0$ for all t. The simplest ones are straight lines or points and, when they are points, their coordinates are

$$x_0 = \frac{2i-1}{2k}, \quad y_0 = \frac{2j-1}{2k}, \quad i,j = 1,2,\ldots,k; \quad k = m,n. \tag{4.2}$$

The number of such points is less than or equal to m^2+n^2 for given m and n. If we introduce local polar coordinates at each point (x_0, y_0), i.e. let

$$x = \frac{2i-1}{2m} + R_0 \cos\phi, \quad y = \frac{2j-1}{2m} + R_0 \sin\phi, \tag{4.3}$$

then substituting (4.3) in (4.1) and letting $\eta = 0$, we have expressions for the nodal curves as they move as a function of time, i.e. we have travelling waves. For R_0 not very small, these curves are expressible in terms of infinite series with Bessel functions as coefficients. For R_0 very small, however, η can be approximated locally by

$$\eta = m\pi R_0 a_2 \left[(-1)^i \alpha \sin t \cos\phi \cos\frac{n\pi(2j-1)}{2m} + (-1)^j \sin(t+\psi)\sin\phi \cos\frac{n\pi(2i-1)}{2m}\right], \tag{4.4}$$

where $\alpha = a_1/a_2$ and $\psi = \theta_2 - \theta_1$, and when $\eta = 0$, we have

$$\tan\phi = C\frac{\sin t}{\sin(t+\psi)}, \qquad \dot{\phi} = \frac{C\sin\psi\cos^2\phi}{\sin^2(t+\psi)}, \tag{4.5}$$

where

$$C = (-1)^{i+j+1}\alpha\frac{\cos\dfrac{n\pi(2j-1)}{2m}}{\cos\dfrac{n\pi(2i-1)}{2m}}. \tag{4.6}$$

We note that, in addition to straight lines as standing waves and their degenerate forms as points given by (4.2), additional degenerate standing waves occur when ϕ is constant, and they occur when $\psi = 0$, i.e. when $\theta_2 = \theta_1$. These are the waves indicated by MS1 and MS2 in the above analysis.

Furthermore, when $\psi = \frac{1}{2}\pi$ and $C = 1$, we note that $\dot{\phi}$ is constant; and thus, locally, these are travelling waves rotating about the nodal points with constant angular velocity. Such waves occur in the degenerate case RM1 and RM2 discussed above. In the more general mixed-mode case GRM, when ψ is arbitrary, we note that $\dot{\phi}$ is of one sign and thus there are rotating waves, but the rotation rate has, in general, a strong second harmonic.

The above discussion is limited to the cases where a_1, a_2, θ_1 and θ_2 are constants, i.e. for constant solutions of (2.27). If these quantities are going through Hopf bifurcations, period-doubling sequences or if they get chaotic, such behaviour will manifest itself as slow-time modifications of the above wave phenomena.

5. Experiments

Experiments were done to check the major conclusions of the theory, regarding the types of periodic and quasi-periodic motions, their amplitudes and the detuning frequency at which they occur. Although we have also observed chaotic behaviour for parameter values at which they are to be expected, the equipment available is inadequate for a detailed study of these phenomena. We refer to the work by Simonelli & Gollub (1989) mentioned in the introduction for the study of these phenomena and also for a much more complete examination of some of the phenomena that we describe here.

The container and some of the equipment are similar to that described by Virnig, Berman & Sethna (1987). The container is of Plexiglas with a horizontal cross-section that is 177.80 mm (7 in.) in one dimension and the other dimension is adjustable to any dimension to produce an almost square container with any desired aspect ratio. Tap water, with Kodak Photo-Flo 200 solution added at a concentration of 1/1000, is used as the fluid. This additive is used to reduce surface tension.

To measure the wave amplitude two simple resistive transducers consisting of pairs of stainless steel rods 3.18 mm ($\frac{1}{8}$ in.) apart and inserted vertically at the linear nodal points are used. The resistance of the fluid between the rods, as it changes with the fluid height, is measured by a Wheatstone bridge arrangement along with Tektronix oscilloscopes using approximately 25 kHz signal. Although there is interference between the transducers, since the Tektronix signals differ by 220 Hz and since the signals measured are at less than 5 Hz, a low-pass filter effectively eliminates the interference. The signal from the Tektronix oscilloscopes is sent to a Norland Prowler dual channel digital oscilloscope. Its built-in function can read the

peak-to-peak value of the signal. This reading is sent to an HP 86/87 microcomputer and recorded on a disk. Because of the time needed for data transmission, The Prowler unit can take only one reading in about a second, while the wave motion itself has a frequency of about 3 Hz. This causes no difficulty, however, since the motion, even when amplitude modulated, is on a very slow timescale. By interpolation of the data, we obtain a smooth function of amplitudes as a function of time. The above measurement system is calibrated with micrometers, as in Virnig *et al.* (1987), before each experiment.

An MTS machine (model 810) is used to provide the vertical sinusoidal excitation. Its built-in feedback control allows us to control the amplitude with a fluctuation of 1%. The forcing frequency is controlled by an HP3310B function generator, which provides the signal to the MTS machine. An HP5315A universal counter is used to display the frequency. After approximately half an hour for warm-up, the frequency drift is less than 0.1% for any ten-minute interval and 0.5% for an eight-hour interval. The harmonic content of the MTS machine is analysed by taking its built-in displacement transducer signal into an HP3582A spectrum analyser. The relative magnitude of high harmonics decreases as the forcing amplitude is increased. For the smallest amplitude we used (1.00 mm peak-to-peak), the second, third and fourth harmonics are 4.84%, 2.90%, 0.66% of that of the fundamental frequency. This can be a source of error and precautions were taken to make sure that the harmonics do not couple with natural frequencies of other modes.

A typical experiment proceeds as follows: First, we select the mode number. Although experiments were done with several mode numbers, (1, 0) and (0, 1) are the most suitable, for easy visualization and for frequency separation, and all the data presented are for these modes. We find that the forcing amplitude has to be less than 2.00 mm, so that the wave amplitudes are not too large (less than 15% of the size of the container). On the other hand, the forcing amplitude has to be above a certain value to be able to see any waves at all. Once the forcing amplitude is decided, we choose the aspect ratio by moving the movable side.

With a given forcing amplitude, we fine tune the frequency to get different wave phenomena. With a fixed forcing amplitude, although σ and β both depend on the frequency, since the change in β is small as a function of the frequency, it is possible to obtain experimentally bifurcation diagrams that are qualitatively the same as those in figures 2–4. The theory curves given in figures 5 and 6 are all for a damping coefficient four times that obtained from the theory of Miles (1967) since this value gives a better fit with the experiments. A comparison with theory results based on damping using Miles formula, however, were still quite acceptable and showed no qualitative features different from those presented here.

To check the theoretical results given on figure 3 for ($\beta_2 < \beta < \beta_3$) a container with a cross-section of 177.8 mm × 180.34 mm (7 in. × 7.1 in.) and a forcing amplitude of 1.00 mm is used. The results are given on figure 5. Starting with a relatively high excitation frequency, as the frequency is decreased we first see one-mode motions corresponding to OM1 and the agreement with theory is good. We note that the wave amplitude at the other transducer is small but not zero. This also is in agreement with the theory. As the frequency is reduced further, the wave motion is a travelling mixed-mode wave corresponding to the theoretical results indicated as RM1. The agreement here with theory is not very good since the theory curve is very steep. With further reduction in frequency, we have single-mode motions OM3 for a_2 and, as before, we have some small signals from the other transducer. Further reduction in frequency gives mixed-mode standing waves MS1. Here the agreement between

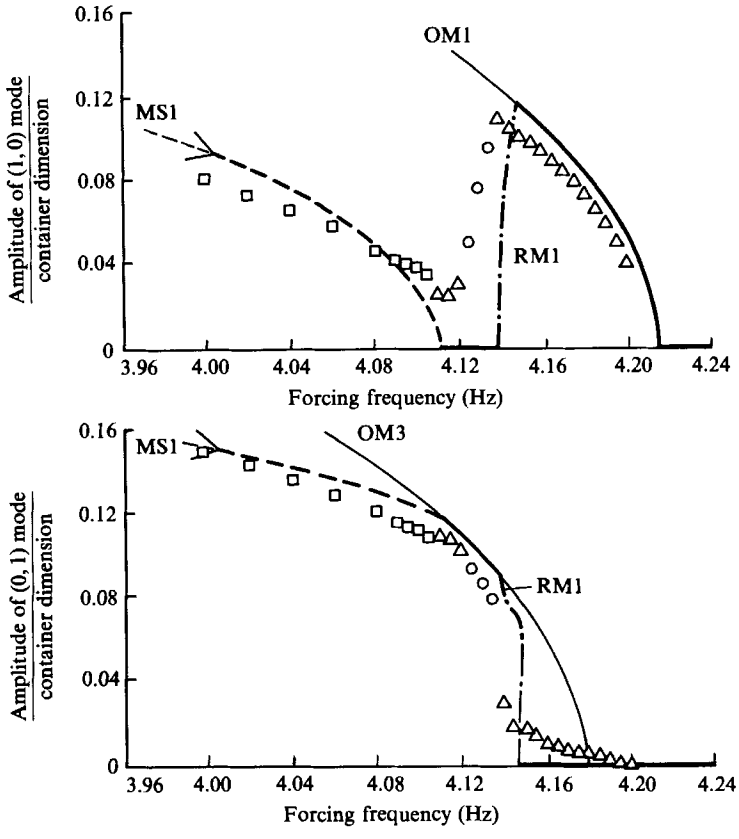

FIGURE 5. Experimental verification of bifurcation diagram on figure 3 for $\beta_2 < \beta < \beta_3$, with the same notation as that in figure 3 for theory curves. The notation for experimental data is: □, standing wave; ○, rotational wave; △, pure one-mode.

theory and experiment is quite good. A further decrease in frequency leads to a region of Hopf bifurcation of MS1 and a potential for chaotic behaviour. Chaotic behaviour of the amplitudes a_1 and a_2 as a function of time was observed at the appropriate frequency values.

On figure 6, we give experimental results corresponding to the bifurcation diagram on figure 3 with $\beta_3 < \beta < \beta_1$. The data are taken with a container cross-section 177.80 mm × 190.50 mm (7 in. × 7.5 in.) and excitation amplitudes 1.25 mm. Starting with a relatively high frequency, as the frequency is reduced we have one-mode motions corresponding to OM1 and, as before, a reading from the other transducer. As the frequency is further reduced, the theory predicts steady travelling waves RM1 as well as two Hopf bifurcations, as shown in figure 3. What is actually observed is some remarkable behaviour with rotating travelling waves with amplitude modulation. We first note that the extremely slow phenomena we describe below occur when the vertical excitation period is about 0.25 s. The wave motion observed is a rotating travelling wave in one direction with a varying amplitude that lasts between 50 and 150 s, depending on the excitation amplitude, until it becomes a pure one-mode motion corresponding to the higher of the two frequencies (OM1). After that, the motion reverses in direction as a rotating travelling wave, which again lasts for about 50 to 150 s. What is plotted on figure 6 is the 'average' amplitude observed

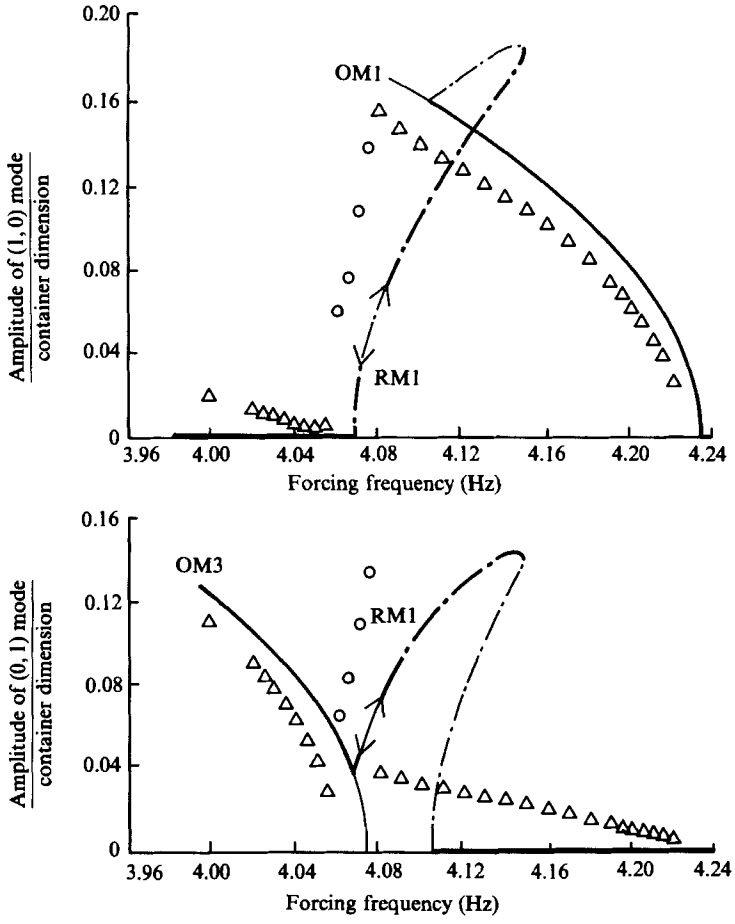

FIGURE 6. Experimental verification of bifurcation diagram on figure 3 for $\beta_3 < \beta < \beta_1$, with the same notation as that in figure 3 for theory curves. The notation for experimental data is: ○, rotational wave; △, pure one-mode.

during this phenomenon at the indicated excitation frequency. The whole phenomenon is very striking and occurs on a timescale that one would associate with Hopf bifurcations. Th phenomenon was definitely not periodic and appeared chaotic, but, because of the extremely long time intervals, a claim of chaotic behaviour is not made here. With further reduction in frequency, pure one-mode motions corresponding to OM3 are observed.

Additional experimental data, not presented here, are obtained that correspond to the bifurcation diagram on figure 4. The theory curves here are similar to those on figure 6, except that here is only one Hopf bifurcation on RM1 and there is a frequency interval when there are no wave motions. The experimental results obtained are very similar to those described for figure 6, including the slow rotation phenomena.

6. Comparison with the results of Simonelli & Gollub

We first note that equations (2.3) of Simonelli & Gollub (1989, hereinafter referred to as S & G), derived from symmetry considerations, are equivalent to our (3.2)

derived from basic principles of fluid mechanics and, in our case, it is possible to give explicit expressions (2.14) and (2.15) for the parameters. We shall attempt here a comparison of our results with those of S & G. We shall limit the discussion to those aspects that pertain to local bifurcations since we in our work touch only slightly on non-local phenomena.

The experimental work of S & G is presented in terms of the physical excitation frequency and amplitude while our results are presented in terms of the dimensionless parameters σ and β. The parameter σ is a function of the detuning of the external excitation, excitation amplitude and the aspect ratio, and when the latter two are constants it is proportional to the detuning. The parameter β is a function of the deviation of the aspect ratio from unity and the excitation amplitude, and for a fixed value of the latter it is proportional to the former. Because of this difference of presentation direct comparison is difficult.

A valid and detailed comparison is possible, however, in the case of the results of S & G for a square container and our results for β small. This is because $\beta = 0$ for the case of a square container when the excitation amplitude is not zero.

The terminology in S & G and that used here is of course different. In S & G 'flat surface', 'pure state' and 'mixed state' correspond to our 'zero solution', 'one-mode solution' (OM) and 'standing wave' (MS) respectively. Taking this difference in terminology into account, we can make a comparison of the experimental results of S & G as given on their figure 4 with our results given on the bifurcation diagram on figure 2 for β small. Our diagram is for a fixed excitation amplitude chosen with a view to give a complete picture of the phenomena. Consider figure 4 of S & G at a fixed excitation amplitude between 150 and 160 μm. Then starting with an excitation frequency of 14.3 and decreasing it gradually we pass through region D of 'pure states' which corresponds to stable parts of our OM1 and OM3 on figure 2. When the frequency is further reduced to reach region C of 'mixed or pure states' they correspond in our figure 2 to the coexistence of standing waves MS1 and OM3 when σ is small and positive. When the frequency is further reduced to reach region B, the 'mixed state' of S & G, we have only MS1 with $\sigma < 0$, as the stable state. With further reduction in frequency we have region A with coexistence of 'mixed state', our MS1 and the 'flay state', our zero solution.

A direct comparison of experimental results of S & G with our results for non-square containers is not possible. It appears, however, that the experimental results on figure 9 of S & G compare fairly well with our results for $\beta > 1$ given on figure 4. Specifically we do not have MS standing waves and S & G do not find coexistence of pure modes, and both works show clear separation of pure states, i.e. our OM1 from OM3.

The main differences between their results and ours lies in the fact that we predict and observe travelling waves and they do not have any evidence of such waves.

The discussion in S & G of figures 5, 6, 7 and 10 is in agreement with our results.

7. Conclusions

We have presented a study of wave motions in a nearly square container under vertical excitations based on the study of a derived set of a fourth-order system of ordinary differential equations, the normal form equations. We give a complete analysis of bifurcation phenomena for almost all values of the system parameters

without having to resort to numerical calculations. We also give experimental verification, although limited in scope but adequate to verify most of the phenomena predicted by the theory. Furthermore, we present experimental evidence of what appears to be interesting chaotic behaviour at values of system parameters at which the theory anticipates such behaviour. A forthcoming study of the same problem for global bifurcations will bring a more complete understanding of this problem.

This work was supported by Grant NSF 0631-5392. The authors wish to acknowledge help from Dr X. M. Gu with some preliminary calculations of the normal form equations and from Mr John Virnig and Mr Marek Behr with some of the experimental work.

REFERENCES

BENJAMIN, T. B. & URSELL, F. 1954 The stability of the plane free surface of a liquid in vertical periodic motion. *Proc. R. Soc. Lond.* A **255**, 505–517.

BRIDGES, T. J. 1987 Secondary bifurcation and change of type of three-dimensional standing waves in a finite depth. *J. Fluid Mech.* **179**, 137–153.

CHOW, S.-N. & HALE, J. K. 1982 *Methods of Bifurcation Theory*. Springer.

CILIBERTO, S. & GOLLUB, J. P. 1984 Chaotic mode competition in parametrically forced surface waves. *J. Fluid Mech.* **158**, 381–398.

FARADAY, M. 1831 On the forms and states assumed by fluids in contact with vibrating elastic surfaces. *Phil. Trans. R. Soc. Lond.* **121**, 319–346.

GOLUBITSKY, M. & STEWART, I. 1985 Hopf bifurcation in the presence of symmetry. *Arch. Rat. Mech. Anal.* **87**, 107–165.

GOLUBITSKY, M. & STEWART, I. 1986 Hopf bifurcation with dihedral group symmetry: coupled nonlinear oscillators. In *Multiparameter Bifurcation Theory*. Contemporary Mathematics, vol. 56 (ed. M. Golubitsky & J. Guckenheimer), pp. 131–173. American Mathematical Society.

GU, X. M. & SETHNA, P. R. 1987 Resonant surface waves and chaotic phenomena. *J. Fluid Mech.* **183**, 543–565.

GUCKENHEIMER, J. & HOLMES, P. 1983 *Nonlinear Oscillations, Dynamical Systems, and Bifurcations of Vector Fields*. Springer.

HOLMES, P. 1986 Chaotic motions in a weakly nonlinear model for surface waves. *J. Fluid Mech.* **162**, 365–388.

KIT, E., SHEMER, L. & MILOH, T. 1987 Experimental and theoretical investigation of nonlinear sloshing waves in a rectangular channel. *J. Fluid Mech.* **181**, 265–291.

MERON, E. & PROCACCIA, I. 1986*a* Theory of chaos in surface waves: The reduction from hydrodynamics to few-dimensional dynamics. *Phys. Rev. Lett.* **56**, 1323–1326.

MERON, E. & PROCACCIA, I. 1986*b* Low-dimensional chaos in surface waves: Theoretical analysis of an experiment. *Phys. Rev.* A **34**, 3221–3237.

MILES, J. W. 1967 Surface-wave damping in closed basins. *Proc. R. Soc. Lond.* A **297**, 459–475.

MILES, J. W. 1984*a* Internally resonant surface waves in a circular cylinder. *J. Fluid Mech.* **149**, 1–14.

MILES, J. W. 1984*b* Resonantly forced surface waves in a circular cylinder. *J. Fluid Mech.* **149**, 15–31.

MILES, J. W. 1984*c* Nonlinear Faraday resonance. *J. Fluid Mech.* **146**, 285–302.

SETHNA, P. R. & BAJAJ, A. K. 1978 Bifurcations in dynamical systems with internal resonance. *Trans. ASME* E: *J. Appl. Mech.* **45**, 895–902.

SIMONELLI, F. & GOLLUB, J. P. 1989 Surface wave mode interactions: effects of symmetry and degeneracy. *J. Fluid Mech.* **199**, 471–494.

SWIFT, J. W. 1988 Hopf bifurcation with the symmetry of the square. To appear.

VERHULST, F. 1979 Discrete symmetric dynamic systems at the main resonances with applications to axi-symmetric galaxies. *Phil. Trans. R. Soc. Lond.* **290**, 435–465.

VERMA, G. R. & KELLER, J. B. 1962 Three-dimensional surface waves of finite amplitude. *Phys. Fluids* **5**, 52–56.

VIRNIG, J. C., BERMAN, A. S. & SETHNA, P. R. 1987 On three-dimensional nonlinear subharmonic resonant surface waves in a fluid. Part II: Experiment. *Trans. ASME* E: *J. Appl. Mech.* **55**, 220–224.